



**HAL**  
open science

## Wavelength-dependent isotope fractionation in visible light O<sub>3</sub> photolysis and atmospheric implications

Früchtl Marion, Janssen Christof, Taraborrelli Domenico, Gromov Sergey,  
Röckmann Thomas

► **To cite this version:**

Früchtl Marion, Janssen Christof, Taraborrelli Domenico, Gromov Sergey, Röckmann Thomas. Wavelength-dependent isotope fractionation in visible light O<sub>3</sub> photolysis and atmospheric implications. *Geophysical Research Letters*, 2015, 10.1002/2015GL066219 . hal-01358299

**HAL Id: hal-01358299**

<https://hal.sorbonne-universite.fr/hal-01358299v1>

Submitted on 29 Nov 2021

**HAL** is a multi-disciplinary open access archive for the deposit and dissemination of scientific research documents, whether they are published or not. The documents may come from teaching and research institutions in France or abroad, or from public or private research centers.

L'archive ouverte pluridisciplinaire **HAL**, est destinée au dépôt et à la diffusion de documents scientifiques de niveau recherche, publiés ou non, émanant des établissements d'enseignement et de recherche français ou étrangers, des laboratoires publics ou privés.

Copyright



## RESEARCH LETTER

10.1002/2015GL066219

## Key Points:

- Visible light photolysis of O<sub>3</sub> leads to isotope enrichment of the remaining O<sub>3</sub>
- Fractionation in visible light photolysis of O<sub>3</sub> is wavelength dependent
- The wavelength dependence is weaker than predicted by theory

## Correspondence to:

M. Früchtl,  
m.fruechtl@uu.nl

## Citation:

Früchtl, M., C. Janssen, D. Taraborrelli, S. Gromov, and T. Röckmann (2015), Wavelength-dependent isotope fractionation in visible light O<sub>3</sub> photolysis and atmospheric implications, *Geophys. Res. Lett.*, 42, 8711–8718, doi:10.1002/2015GL066219.

Received 16 SEP 2015

Accepted 23 SEP 2015

Accepted article online 29 SEP 2015

Published online 23 OCT 2015

Wavelength-dependent isotope fractionation in visible light O<sub>3</sub> photolysis and atmospheric implications

Marion Früchtl<sup>1</sup>, Christof Janssen<sup>2,3</sup>, Domenico Taraborrelli<sup>4</sup>, Sergey Gromov<sup>4,5</sup>, and Thomas Röckmann<sup>1</sup>

<sup>1</sup>Institute for Marine and Atmospheric Research Utrecht, Utrecht University, Utrecht, Netherlands, <sup>2</sup>LERMA, Observatoire de Paris, PSL Research University, CNRS, UMR 8112, Paris, France, <sup>3</sup>Sorbonne Universités, UPMC Univ Paris 6, UMR 8112, LERMA, Paris, France, <sup>4</sup>Max Planck Institute for Chemistry, Mainz, Germany, <sup>5</sup>Institute of Global Climate and Ecology (Roshydromet and RAS), Moscow, Russia

**Abstract** The <sup>17</sup>O and <sup>18</sup>O isotope fractionation associated with photolysis of O<sub>3</sub> in the Chappuis band was determined using a broadband light source with cutoff filters at 455, 550, and 620 nm and narrowband light sources at 530, 617, and 660 nm. The isotope effects follow a mass-dependent fractionation pattern ( $\delta^{17}\text{O}/\delta^{18}\text{O} = 0.53$ ). Contrary to theoretical predictions, fractionations are negative for all wavelength ranges investigated and do not change signs at the absorption cross-section maximum. Our measurements differ from theoretical calculations by as much as 34‰ in  $^{18}\epsilon_{\text{O}_3+h\nu} = (^{18}J/^{16}J - 1)$ . The wavelength dependence is also weaker than predicted. Photo-induced fractionation is strongest when using a low-wavelength cutoff at 620 nm with  $^{18}\epsilon_{\text{O}_3+h\nu} = -26.9(\pm 1.4)\text{‰}$ . With decreasing wavelength, fractionation values diminish to  $^{18}\epsilon_{\text{O}_3+h\nu} = -12.9(\pm 1.3)\text{‰}$  at 530 nm. Results from an atmospheric model demonstrate that visible light photolysis is the most important tropospheric sink of O<sub>3</sub>, which thus contributes about one sixth to the ozone enrichment.

## 1. Introduction

Ozone (O<sub>3</sub>) carries a strong enrichment (~100‰) in both heavy oxygen isotopes <sup>17</sup>O and <sup>18</sup>O compared to atmospheric O<sub>2</sub> [Mauersberger, 1981; Krankowsky et al., 1995, 2007; Johnson et al., 2000]. This enrichment shows a marked deviation from classical mass-dependent fractionation, where  $\delta^{17}\text{O} \approx 0.52 \times \delta^{18}\text{O}$ . Mass-independent isotope fractionation can be quantified by the <sup>17</sup>O excess

$$\Delta^{17}\text{O} = \delta^{17}\text{O} - 0.52 \times \delta^{18}\text{O}. \quad (1)$$

The peculiar high enrichments in the heavy isotopes <sup>17</sup>O and <sup>18</sup>O originate from the O<sub>3</sub> formation reaction [Krankowsky et al., 1995; Johnson et al., 2000; Mauersberger et al., 2001] and strongly depend on temperature and pressure [Morton et al., 1990; Thiemens and Jackson, 1990; Krankowsky et al., 2007]. In addition, atmospheric studies suggested a contribution of processes other than O<sub>3</sub> formation to the observed isotope enrichments in atmospheric O<sub>3</sub>. At altitudes above 30 km atmospheric fractionations were between 35 and 40‰ higher than what is expected from the known isotope effects in O<sub>3</sub> formation [Haverd et al., 2005; Krankowsky et al., 2007]. The observed additional enrichment was tentatively attributed to the process of O<sub>3</sub> photolysis.

A semianalytical theory to calculate photolysis-induced isotope effects in O<sub>3</sub> and other gases [Miller and Yung, 2000; Miller et al., 2005; Liang et al., 2006] predicts pronounced wavelength-dependent isotope effects during photolysis. In the Chappuis band (400–800 nm) calculated fractionations show significantly nanometer-scale variability superimposed on a general trend from positive fractionation on the short-wavelength side of the absorption maximum to strongly negative fractionation at the long-wavelength tail [Liang et al., 2006]. Ndengué et al. [2010, 2012, 2014] performed improved calculations of isotope-specific absorption cross sections, using quantum mechanical multiconfiguration time-dependent Hartree wave packet propagation on ab initio surfaces, but the cross sections are not provided, which impedes direct comparison. For both types of calculation, model results show that the photolysis-induced isotope effects contribute significantly to the isotopic composition of O<sub>3</sub> in the atmosphere [Liang et al., 2006; Ndengué et al., 2014]. While Ndengué et al. [2014] claim a strict mass dependence for O<sub>3</sub> photodissociation, the results of their atmospheric calculations show a <sup>17</sup>O excess of 2.5 to 3.5‰ at altitudes up to 32 km. If these numbers are significant, they will imply a non-mass-dependent isotope fractionation from photolysis in the Huggins and/or Chappuis bands.

Due to the inherent approximations in the theoretical treatments, experimental studies are required to provide benchmark data. *Morton et al.* [1990] reported no significant change in  $O_3$  when photolyzed with visible light, whereas *Chakraborty and Bhattacharya* [2003] found a mass-dependent fractionation pattern ( $\delta^{17}O/\delta^{18}O = 0.54$ ) for photolysis of  $O_3$  at 520 nm and 630 nm. The fractionation coefficients they obtained for both wavelengths showed similar values of  $^{18}\epsilon_{O_3+h\nu} = -13.7 \pm 2\%$  and  $^{17}\epsilon_{O_3+h\nu} = -7.25 \pm 0.1\%$ . However, the calculations by *Liang et al.* [2006] yielded very different fractionations for photolysis at the two wavelengths,  $^{18}\epsilon_{O_3+h\nu} = +5.8\%$  at 520 nm and  $^{18}\epsilon_{O_3+h\nu} = -31\%$  at 630 nm (average values for the symmetric and asymmetric isotopomers).

A complication of the above photolysis experiments using pure  $O_3$  samples is that the O atom that is produced during photolysis generally destroys another  $O_3$  molecule in the reaction  $O + O_3$ . Thus, isotope effects in photolysis and chemical removal cannot be disentangled [*Brenninkmeijer et al.* 2003]. *Früchtl et al.* [2015] combined photolysis experiments of pure  $O_3$  and  $O_3$  mixed in a large excess of CO, which acts as O atom quencher, to separately quantify the fractionation in both removal processes. Photolysis experiments using a broadband light source with a 455 nm long-pass filter yielded  $^{18}\epsilon_{O_3+h\nu} = -16.1(\pm 1.4)\%$  and  $^{17}\epsilon_{O_3+h\nu} = -8.05(\pm 0.7)\%$ , and  $^{18}\epsilon_{O_3+O} = -11.9(\pm 1.4)\%$  and  $^{17}\epsilon_{O_3+O} = -5.95(\pm 0.7)\%$ . Notably, both fractionations are mass dependent.

Following up on these results, we examine here the (low-resolution) wavelength dependence of the isotope fractionation in the photolysis of  $O_3$  by visible light using various light sources and cutoff filters.

## 2. Methods

### 2.1. Experimental Procedure

The experimental system has been described in detail in *Früchtl et al.* [2015].  $O_3$  was produced by electric discharge from  $\sim 8.0$  hPa of pure  $O_2$  (99.9998%) in a spherical 1.0 L glass reactor with a cylindrical extension immersed in liquid nitrogen ( $LN_2$ ).  $O_3$  condensed at the reactor wall, and the remaining  $O_2$  was pumped away. Subsequently,  $O_3$  was brought to room temperature, and an aliquot was expanded to the cylindrical photolysis chamber ( $V = 630 \text{ cm}^3$ ) for photolysis. After photolysis, the leftover  $O_3$  was separated from  $O_2$  by pumping the mixture through a cryogenic trap cooled to the triple-point temperature of  $N_2$  (63 K). At this temperature  $O_3$  condenses but  $O_2$  produced during photolysis does not and can be pumped away. The collected  $O_3$  was transferred to a sample bottle ( $V = 44 \text{ cm}^3$ ) containing molecular sieve (13X) immersed in  $LN_2$  and subsequently converted to molecular  $O_2$  by heating. The amount of  $O_2$  originating from  $O_3$  was then determined by measuring the pressure after transfer to a reference volume ( $V = 1.8 \text{ cm}^3$ , containing molecular sieve). The isotopic composition was determined on a Dual Inlet isotope ratio mass spectrometer (IRMS) (Thermo Finnigan Delta Plus XL) with an uncertainty of  $0.03\%$  for  $\delta^{18}O$  and  $0.08\%$  for  $\delta^{17}O$  ( $n = 150$ ).

Two sets of photolysis experiments were conducted. In the first set, a broadband light source ( $\lambda = 400$  to  $800$  nm) with an emission peak at  $605$  nm was used (tungsten halogen lamp, Osram HLX 64633, described in *Früchtl et al.* [2015]). To select different wavelength regions, we used different optical long-pass glass color filters with cutoff wavelengths at  $455 \pm 6$ ,  $550 \pm 6$ , or  $620 \pm 5$  nm (GG455, OG550, Schott; R-620, Hoya). For each experiment the corresponding filter was placed between the lamp and the photolysis chamber. In the second set, three narrowband light sources (high-power light-emitting diodes (LEDs)) with emission peaks at  $530$ ,  $617$ , and  $660$  nm and respective bandwidths (full width at half maximum) of  $33$ ,  $18$ , and  $25$  nm were used (Thorlabs M530L3, M617L3, and M660L3).

Each experiment consisted of measuring three aliquots from the same initial  $O_3$  reservoir. The first aliquot expanded into the photolysis chamber was used as control measurement to correct for small  $O_3$  losses that occur without photolysis. The second aliquot (expansion #2) was collected after 10 to 30 min of photolysis. The final aliquot (expansion #3) is the residual  $O_3$  in the discharge reactor, which represents the original  $O_3$  produced in the electric discharge.

In the following we refer to the amount of the photolyzed sample (expansion #2, corrected for the control experiment) as  $O_3(\text{end})$  and the remaining  $O_3$  from the discharge reactor (expansion #3) as  $O_3(\text{start})$ . The remaining fraction  $f(O_3)$  after a certain time  $t$  of photolysis is defined as  $f(O_3) = O_3(\text{end})/O_3(\text{start})$ . Isotope enrichments are reported as  $\delta^xO = (N(^xO)/N(^{16}O))_{SA}/(N(^xO)/N(^{16}O))_{ST} - 1$ , where  $x$  indicates heavy isotope

**Table 1.** Overview of Measurement Results Compared to Liang *et al.* [2006]

	$J(\text{s}^{-1}) (\times 10^{-4})$	$\varepsilon(\text{total})$ (‰)		$(\varepsilon_{\text{O}_3+h\nu})$ (‰)		$\varepsilon_{(\text{O}_3+h\nu)\text{Liang et al.}}$ (‰)	
		$^{18}\text{O}$	$^{17}\text{O}$	$^{18}\text{O}$	$^{17}\text{O}$	$^{18}\text{O}$	$^{17}\text{O}$
455 nm filter	3.34 ( $\pm 0.06$ )	-14.1 ( $\pm 0.2$ )	-7.5 ( $\pm 0.1$ )	-16.2 ( $\pm 1.1$ )	-8.9 ( $\pm 0.6$ )	-9.6	-5.1
550 nm filter	2.69 ( $\pm 0.07$ )	-13.5 ( $\pm 0.5$ )	-7.1 ( $\pm 0.3$ )	-15.2 ( $\pm 1.3$ )	-8.3 ( $\pm 0.9$ )	-14.0	-7.4
620 nm filter	1.18 ( $\pm 0.08$ )	-19.4 ( $\pm 0.6$ )	-10.2 ( $\pm 0.2$ )	-26.9 ( $\pm 1.4$ )	-14.4 ( $\pm 1.0$ )	-34.0	-17.9
530 nm LED	0.89 ( $\pm 0.03$ )	-12.4 ( $\pm 0.4$ )	-6.7 ( $\pm 0.3$ )	-12.9 ( $\pm 1.3$ )	-7.5 ( $\pm 0.8$ )	20.9	10.9
617 nm LED	3.33 ( $\pm 0.07$ )	-13.4 ( $\pm 0.2$ )	-7.2 ( $\pm 0.1$ )	-15.0 ( $\pm 1.1$ )	-8.4 ( $\pm 0.6$ )	-1.5	-0.7
660 nm LED	2.86 ( $\pm 0.15$ )	-17.9 ( $\pm 0.3$ )	-9.5 ( $\pm 0.2$ )	-23.9 ( $\pm 1.2$ )	-13.1 ( $\pm 0.7$ )	-21.8	-11.4

mass numbers 18 or 17. The  $\delta$  quantifies the relative deviation of the ratio  $N(^X\text{O})/N(^{16}\text{O})$  of isotope abundances ( $N$ ) in a sample (SA) from the same ratio in a standard material (ST). Values are reported in per mill (‰). The isotopic composition of initial  $\text{O}_3$  is chosen as standard.

## 2.2. Photolysis Rate and Fractionations in $\text{O}_3$ Photolysis

The photolysis rate  $J$  is determined from the temporal evolution of  $\text{O}_3$  removal ( $f$ ) in the experiments

$$J = 0.5 \ln(f)/t. \quad (2)$$

Measured photolysis rates range from  $3.3(\pm 0.06) \times 10^{-4} \text{ s}^{-1}$  (455 nm filter) to  $0.9(\pm 0.03) \times 10^{-4} \text{ s}^{-1}$  (530 nm LED) (Table 1). The spectral photolysis rate for each light source is shown in Figure 2a. Values are calculated by multiplying  $\text{O}_3$  absorption cross sections [Sander *et al.*, 2011] with the spectral actinic flux under the assumption of unit quantum yield. The spectral actinic flux with different filters was obtained by multiplication of the actinic flux of the halogen lamp without filter (determined with a spectral photometer, model 752, Optronic laboratories Inc., USA) with the filter internal transmittance published by the manufacturer. For LED light sources, the spectral actinic flux data provided by the manufacturer were used.

## 2.3. Control Measurements and Error Estimates

The stability of the analytical system was characterized by *control* measurements without irradiation as described above. A loss of 4–7% of  $\text{O}_3$  was observed in the control experiments, associated with changes of  $\delta^{18}\text{O} < 0.1\text{‰}$  and  $\delta^{17}\text{O} < 0.05\text{‰}$ . For correction, average values from the control measurements were subtracted from the raw data of the photolysis experiments.

Uncertainty estimates for  $\delta^{18}\text{O}$  and  $\delta^{17}\text{O}$  include errors from control measurements ( $\sigma_{\text{control}}$ ) and IRMS measurements ( $\sigma_{\text{O}_3 \text{ end}}, \sigma_{\text{O}_3 \text{ start}}$ ) according to

$$\sigma = \sqrt{(\sigma_{\text{O}_3 \text{ end}})^2 + (\sigma_{\text{O}_3 \text{ start}})^2 + (\sigma_{\text{control}})^2}; \quad (3)$$

total errors are  $< 0.2\text{‰}$  for  $^{17}\text{O}$  and  $^{18}\text{O}$ .

Uncertainties in  $\ln(f)$  as a consequence of the applied sampling procedure were derived from experiments with pure  $\text{CO}_2$  instead of  $\text{O}_3$ , because  $\text{CO}_2$  is easy to trap and transfer in vacuum systems with virtually no loss ( $> 99.5\%$  recovery). Considering a small nonlinearity of the pressure sensor, errors in pressure reading, and small changes in temperature, total relative uncertainties in  $\ln(f)$  are between 2.6 and 2.8% [Früchtl *et al.*, 2015].

## 3. Results

Figures 1a–1d show that, independent of the light source used, the remaining  $\text{O}_3$  becomes isotopically enriched during the photolysis experiments; i.e., the heavy isotopologues are removed more slowly than  $^{16}\text{O}_3$  for all wavelength ranges. The measured fractionations  $\varepsilon$  for  $^{18}\text{O}$  vary between  $-12.4\text{‰}$  and  $-19.4\text{‰}$  and between  $-6.7\text{‰}$  and  $-10.2\text{‰}$  for  $^{17}\text{O}$  (Figures 1b and 1d and Table 1).  $\text{O}_3$  photolysis with the broadband lamp using a 550 nm or a 455 nm filter or the 617 nm LED result in very similar fractionations (Table 1). For these experiments the peak emission is slightly above 600 nm. The fractionations become more negative toward longer wavelength (620 nm filter, 660 nm LED). At shorter wavelength (530 nm), the fractionation values are highest but still clearly negative at  $^{18}\varepsilon = -12.4\text{‰}$  and  $^{17}\varepsilon = -6.7\text{‰}$ .

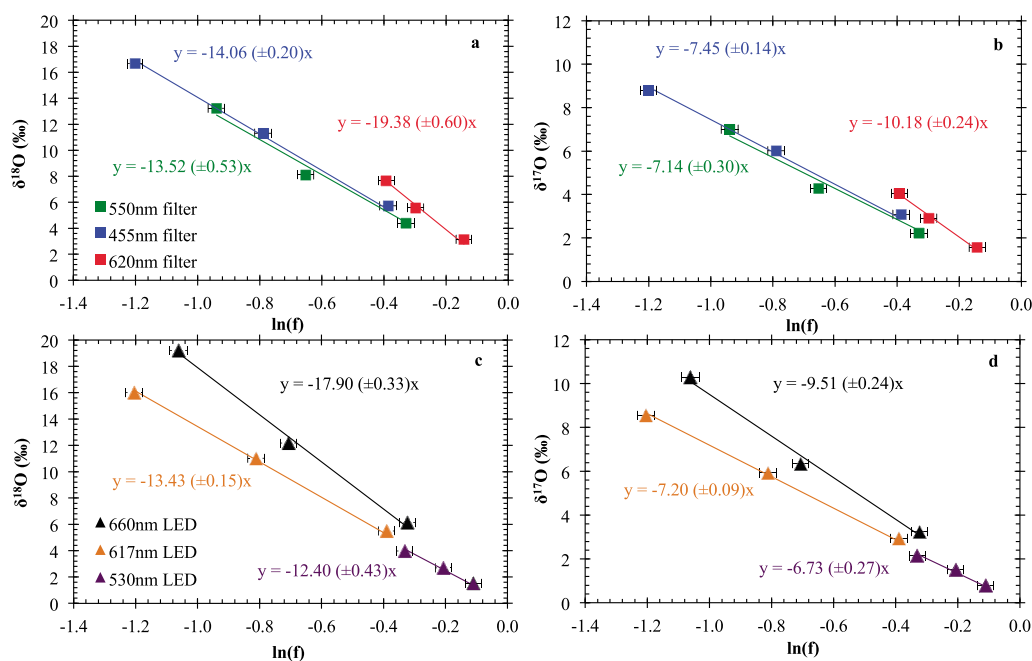
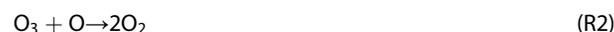


**Figure 1.** Rayleigh fractionation plots for O<sub>3</sub> photolysis experiments of 10, 20, and 30 min (three points in each series). (a and b) Photolysis with the halogen lamp and different filters. (c and d) Photolysis with high-power LEDs. δ<sup>17</sup>O and δ<sup>18</sup>O are given versus O<sub>3</sub>(start). Errors in the slopes (ε<sub>total</sub>) are based on least squares fits forced through zero. Errors in ln(f) are between 0.026 and 0.028. Errors in δ values are < 0.2‰.

As mentioned above, the observed fractionation in the photolysis experiments with pure O<sub>3</sub> does not only include O<sub>3</sub> photolysis (R1) but, due to the photolytic production of O atoms, also the chemical O<sub>3</sub> removal via (R2).



In our experiments the rates of O<sub>3</sub> photolysis (R1) and O<sub>3</sub> + O (R2) are very similar and reformation of O<sub>3</sub> via (R3) is negligible (<1%). These conclusions are in line with isotope kinetic modeling (not shown). Thus, the total fractionation (ε<sub>total</sub>) is the average of the two fractionations in reactions (R1) and (R2)

$$\epsilon_{total} = (\epsilon_{O_3+h\nu} + \epsilon_{O_3+O})/2. \tag{4}$$

Using the previously determined fractionation values for (R2) of <sup>18</sup>ε<sub>O<sub>3</sub>+O</sub> = -11.9(±1.4)‰ and <sup>17</sup>ε<sub>O<sub>3</sub>+O</sub> = -5.95(±0.7)‰ [Früchtl et al., 2015], the photolysis-induced fractionations can be calculated from equation (4).

The resulting fractionations attributed to O<sub>3</sub> photolysis are shown in Table 1 and Figures 2b and 2c. For all the wavelength intervals investigated, photolysis of O<sub>3</sub> induces negative fractionations, with a trend to stronger isotopic fractionation at longer wavelengths. Measured fractionations range between -26.9‰ and -12.9‰ for <sup>18</sup>O and -14.4‰ and -7.5‰ for <sup>17</sup>O in experiments applying a 620 nm filter or the 530 nm LED, respectively. Figure 2 also shows the wavelength-dependent fractionations calculated by Liang et al. [2004, 2006]. By convolving these fractionations with the photolysis spectra of our light sources, the predicted photo-induced fractionations for our experimental conditions were calculated (Table 1 and Figures 2b and 2c).

The theoretical predictions agree best with the experiments using the broadband lamp with 550 nm filter or 660 nm LED, with maximum differences of only 3.3‰ for <sup>18</sup>ε<sub>O<sub>3</sub>+hν</sub> and 1.8‰ for <sup>17</sup>ε<sub>O<sub>3</sub>+hν</sub>. In qualitative agreement with calculations [Liang et al., 2006] we observe a wavelength dependence and stronger

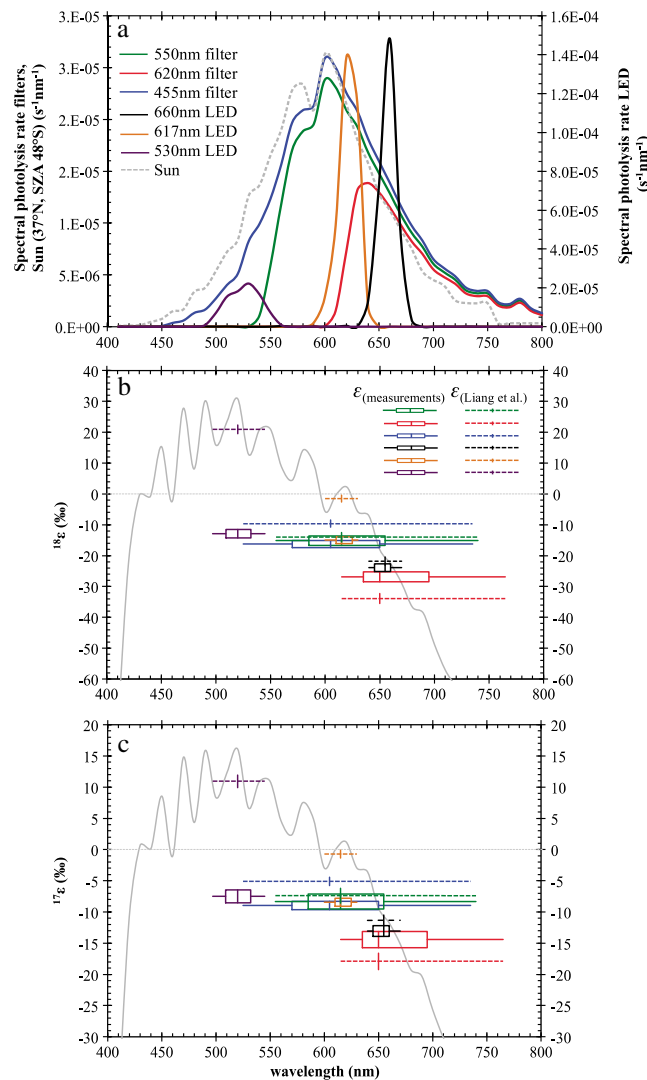


**Figure 2.** (a) Spectral photolysis rates for the different light sources used in the experiments. Green: 550 nm filter, red: 620 nm filter, blue: 455 nm filter, orange: 617 nm LED, black: 660 nm LED, purple: 530 nm LED, grey (dashed): Sun (37°N, SZA 48°S, from <http://rredc.nrel.gov/solar/spectra/am1.5/>). Filter and LED data are scaled to the measured photolysis rate  $J$  of each light source (section 2.2), whereas the Sun spectrum is scaled to  $J_{455\text{nm filter}}$ . (b and c) Isotope fractionations  $^{18}\epsilon$  and  $^{17}\epsilon$ . Colors represent different filter and LEDs as defined in Figure 2a. The box width and solid horizontal lines indicate the wavelength intervals in which 50% and 90%, respectively, of the photons are emitted. Solid vertical lines indicate the medians. The height of the boxes marks the error for  $\epsilon_{\text{O}_3+h\nu}$  calculated as  $\sigma_{\text{O}_3+h\nu} = \sqrt{(2 \times \sigma_{\epsilon(\text{total})})^2 + (\sigma_{\epsilon(\text{O}+\text{O}_3)})^2}$ . The grey solid lines show the wavelength-dependent fractionations as calculated by Liang et al. [2004, 2006]. The dashed lines show the fractionations expected from theoretical calculations by Liang et al. for our light sources.

between our measurements and the theoretical calculations by Liang et al. [2006], which predict positive fractionations for  $\lambda < 600$  nm, cannot be attributed to erroneous assumptions in  $\epsilon_{\text{O}_3+\text{O}}$ .

Isotope effects in  $\text{O}_3$  photolysis result from variations of the transition dipole moment (TDM) with isotopic substitution [Schinke, 1993]. Since the semiempirical zero-point energy approach is based on the main isotopologue only, variations in TDM with isotopic substitution cannot be predicted accurately. For photolysis of

fractionations at longer wavelengths. At shorter wavelengths, however, the observed wavelength dependence is much smaller than predicted and discrepancies become considerable (33.9‰ and 18.5‰ for  $^{18}\epsilon_{\text{O}_3+h\nu}$  and  $^{17}\epsilon_{\text{O}_3+h\nu}$  at 530 nm). Most importantly, the experimentally determined fractionations do not show change in sign toward shorter wavelengths, whereas the calculations predict a change from negative to positive values below 600 nm.

Figure 3 shows the three-isotope plot ( $\delta^{17}\text{O}/\delta^{18}\text{O}$ ) for all photolysis experiments. There is no significant difference between the three-isotope slopes of individual experiments, and a fit to all data follows a slope of 0.534 ( $\pm 0.003$ ) at a confidence level of 99%, which is in agreement with previous results from Chakraborty and Bhattacharya [2003].

#### 4. Discussion

A possible systematic uncertainty in the experimental determination of the photolysis-induced fractionation is due to the need to correct for the fractionation in the  $\text{O}_3 + \text{O}$  reaction. The correction depends on the results of Früchtl et al. [2015], where unexplained losses of  $\text{O}_3$  might have introduced systematic errors in the determination of  $\epsilon_{\text{O}_3+\text{O}}$ . Estimating the effects of these errors yielded lower limits of  $^{18}\epsilon_{\text{O}_3+\text{O}} = -18.6\text{‰}$  and  $^{17}\epsilon_{\text{O}_3+\text{O}} = -9.3\text{‰}$  [Früchtl et al., 2015]. According to equation (4), lower values associated with  $\epsilon_{\text{O}_3+\text{O}}$  would lead to correspondingly higher values for  $\epsilon_{\text{O}_3+h\nu}$ . However, even for the estimated lower limits for  $\epsilon_{\text{O}_3+\text{O}}$ , the photolysis-induced fractionations  $\epsilon_{\text{O}_3+h\nu}$  would remain negative over all of the wavelength ranges investigated with highest values of  $^{18}\epsilon_{\text{O}_3+h\nu} = -6.2\text{‰}$  and  $^{17}\epsilon_{\text{O}_3+h\nu} = -4.2\text{‰}$ . Therefore, the strong discrepancy

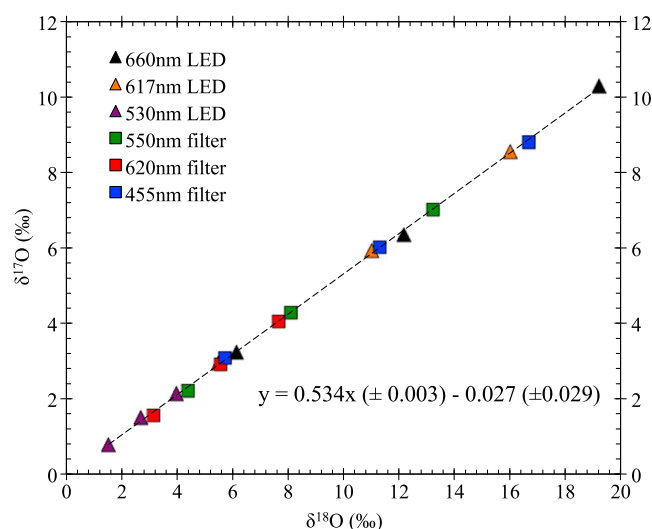


**Figure 3.** Three-isotope plot. Different symbols represent the different sets of experiments. The linear fit has a slope of  $0.534 \pm 0.003$  and a nonsignificant y axis intercept.

$\text{N}_2\text{O}$ , results from ab initio calculations agree better with experimentally determined isotope fractionations than semi-empirical calculations [Schmidt *et al.*, 2011]. For  $\text{CO}_2$ , the ab initio calculations [Schmidt *et al.*, 2013] reported 3 times stronger fractionations than predicted by the semiempirical approach applied by Liang *et al.* [2004]. Furthermore, Ndengué *et al.* [2014] showed that the assumption by Liang *et al.* [2004] of a proportional relationship between changes in absorption cross sections under isotopic substitution and changes in zero point energy for both central and terminal substitution is not valid. This suggests that the discrepancies in magnitude and wavelength dependence between our observations and the theoretical calculations by Liang *et al.* [2004, 2006] are likely to arise

from shortcomings in the semianalytical approach. The observed weak wavelength dependency of  $\epsilon$  is experimentally supported by the results of Chakraborty and Bhattacharya [2003], who found similar fractionations for  $\text{O}_3$  photolysis at  $520(\pm 2)$  and  $630(\pm 4)$  nm, although they could not take into account the  $\text{O}_3 + \text{O}$  reaction.

In order to assess the implications of our results for  $\text{O}_3$  photolysis in the atmosphere, Figure 2a includes the spectral photolysis rate calculated using a typical solar actinic flux spectrum. This spectral photolysis rate is quite similar to that achieved with the broadband photolysis lamp using the 455 nm long-pass filter, with the solar curve being slightly blueshifted. The relatively weak wavelength dependence of the fractionation found in our experiments implicates that the overall fractionation under solar irradiation should be rather similar to the value obtained with the broadband lamp and the 455 nm filter. The blueshift of the solar photolysis rate would result in a slightly larger contribution from the short-wave tail with lower fractionations and a smaller contribution from the long-wave tail with stronger fractionations. Since these tail regions are not well covered by our experiments, precise quantification is not possible at present, but we estimate that the total fractionation in the atmosphere may be a few per mill lower than  $^{18}\epsilon_{\text{O}_3+h\nu} = -16.1 (\pm 1.1)\%$  and  $^{17}\epsilon_{\text{O}_3+h\nu} = -8.9 (\pm 0.6)\%$ , which was found with the broadband lamp and the 455 nm filter (Table 1, 455 nm filter). Compared to a total fractionation of 90‰ observed for atmospheric  $\text{O}_3$  [Frankowsky *et al.*, 2007; Johnston and Thiemens, 1997], the fractionation in visible light  $\text{O}_3$  photolysis is of significant magnitude and needs to be considered when investigating isotope effects of ozone.

Ozone is a highly reactive molecule, and its isotopic composition in the atmosphere is determined by the dynamic balance between isotope fractionation in ozone formation and in its gross loss. In order to quantify the importance of Chappuis band photolysis as gross removal process, we analyzed the turnover of  $\text{O}_3$  in the global model EMAC (ECHAM5/MESy Atmospheric Chemistry, [Jöckel *et al.*, 2006, 2010]). EMAC is equipped with the comprehensive chemical mechanism accounting for all relevant gas phase and photolytic  $\text{O}_3$  reactions [Taraborrelli *et al.*, 2012], further revised and extended with monoterpenes/aromatics chemistry including ozonolysis [Bloss *et al.*, 2005; Hens *et al.*, 2014; Nölscher *et al.*, 2014; Peeters *et al.*, 2014]. The EMAC photolysis submodel [Sander *et al.*, 2014] provides wavelength-resolved photolysis rates and their integrals for the channels leading to  $\text{O}(^3\text{P})$  and  $\text{O}(^1\text{D})$  production. Photolysis in the Huggins band produces  $\text{O}(^3\text{P})$  and yields about 90%  $\text{O}(^1\text{D})$  and 10%  $\text{O}(^3\text{P})$  for the lower stratosphere and below. We diagnose that visible light photolysis in the Chappuis band accounts for more than 85% of the overall  $\text{O}_3$  gross removal rate simulated by EMAC, from the free troposphere up to 50 hPa (Figure 4a). Only in the regions strongly affected by anthropogenic emissions the removal via nonphotolytic sinks (predominantly in  $\text{NO}_x$  and  $\text{HO}_x$  chemistry) is of

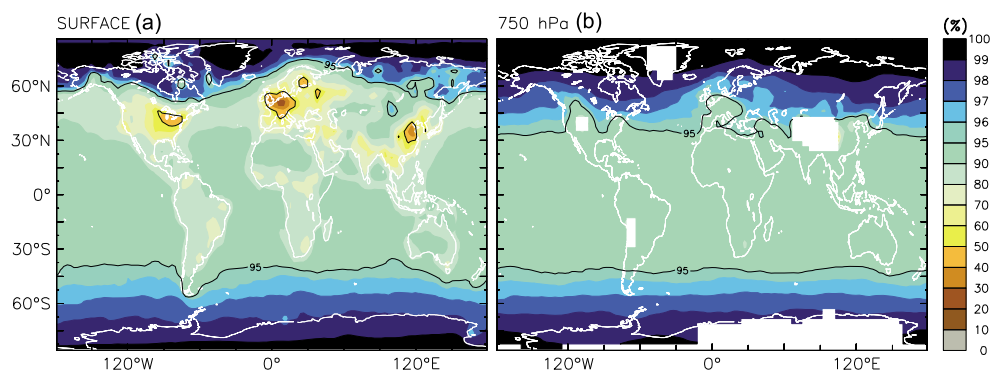


**Figure 4.** Fraction (in per cent) of the total  $O_3$  sink attributed to photolysis leading to  $O_3(P)$  production simulated by EMAC at (a) the surface and (b) 750 hPa pressure layers. Shown is a typical example from March 2001. White areas indicate regions with surface pressures lower than 750 hPa; superimposed contours refer to 50% and 95% levels, respectively.

similar importance as Chappuis band photolysis near the surface (Figure 4b). Above 800 hPa, however, the photolytic sink clearly dominates (Figure 4b). We conclude that the fractionation in Chappuis band photolysis globally affects the isotopic composition of  $O_3$  in the troposphere.

The derived three-isotope slope of  $0.534(\pm 0.003)$  is at the upper end of the range that is usually considered as mass-dependent fractionation, and the value is higher than the one used in the defining equation of  $\Delta^{17}O$  (equation (1)). For  $^{18}e_{O_3+h\nu}$  values of  $-15\text{‰}$  in atmospheric Chappuis band photolysis and a difference of 0.014 from  $^{17}\delta/^{18}\delta = 0.52$  in the three-isotope slope, the corresponding  $\Delta^{17}O$  values would be 0.2 to 0.3‰ (equation (1)). This is 2 orders of magnitude lower than  $\Delta^{17}O$  of atmospheric  $O_3$ , which ranges between 25 and 40‰ [Vicars and Savarino, 2014; Brenninkmeijer et al., 2003; Krankowsky et al., 2007; Johnston and Thiemens, 1997]. Therefore, the contribution of visible light photolysis to the mass-independent isotope signature of atmospheric  $O_3$  could be negligible.

Our results further indicate that previous experiments to determine the isotope fractionation in  $O_3$  formation via photolytic recycling of  $O_3$  in an  $O_2$  bath gas using visible light [Morton et al., 1990] may be biased by non-negligible isotope effects in  $O_3$  photolysis.

Whereas the results from this study suggest shortcomings in the calculation of the overall wavelength dependence of photolysis-induced  $O_3$  fractionation in the Chappuis band, the wavelength resolution of the light sources employed is insufficient to examine smaller-scale (few nanometers and subnanometers) variability that was also predicted by the calculations [Miller et al., 2005; Liang et al., 2006]. Laser light sources could help to investigate this further, but high power is required to realize sufficient removal of  $O_3$  in laboratory experiments.

#### Acknowledgments

The authors gratefully acknowledge support from the Marie Curie Initial Training Network INTRAMIF (Initial Training Network on Mass Independent Fractionation) as part of the European Community's Seventh Framework Program (FP7/2007-2013), grant 237890. We thank Matthew S. Johnson for his comments on the discussion of the model-derived isotope effects in ozone photolysis. The data presented in this paper are available at <http://www.projects.science.uu.nl/atmosphereclimate/Data.php>.

The Editor thanks two anonymous reviewers for their assistance in evaluating this paper.

#### References

- Bloss, C., et al. (2005), Development of a detailed chemical mechanism (MCMv3.1) for the atmospheric oxidation of aromatic hydrocarbons, *Atmos. Chem. Phys.*, *5*(3), 641–664, doi:10.5194/acp-5-641-2005.
- Brenninkmeijer, C. A. M., C. Janssen, J. Kaiser, T. Röckmann, T. S. Rhee, and S. S. Assonov (2003), Isotope effects in the chemistry of atmospheric trace compounds, *Chem. Rev.*, *103*(12), 5124–5162.
- Chakraborty, S., and S. K. Bhattacharya (2003), Oxygen isotopic anomaly in surface induced ozone dissociation, *Chem. Phys. Lett.*, *369*(5–6), 662–667, doi:10.1016/S0009-2614(03)00018-6.
- Früchtl, M., C. Janssen, and T. Röckmann (2015), Experimental study on isotope fractionation effects in visible photolysis of  $O_3$  and in the  $O + O_3$  odd oxygen sink reaction, *J. Geophys. Res. Atmos.*, *1–19*, doi:10.1002/2014JD022944.
- Haverd, V., G. C. Toon, and D. W. T. Griffith (2005), Evidence for altitude-dependent photolysis-induced  $^{18}O$  isotopic fractionation in stratospheric ozone, *Geophys. Res. Lett.*, *32*, L22808, doi:10.1029/2005GL024049.
- Hens, K., et al. (2014), Observation and modelling of  $HO_x$  radicals in a boreal forest, *Atmos. Chem. Phys.*, *14*(16), 8723–8747, doi:10.5194/acp-14-8723-2014.
- Jöckel, P., et al. (2006), The atmospheric chemistry general circulation model ECHAM5/MESy1: Consistent simulation of ozone from the surface to the mesosphere, *Atmos. Chem. Phys.*, *6*, 5067–5104, doi:10.5194/acp-6-5067-2006.
- Jöckel, P., A. Kerkweg, A. Pozzer, R. Sander, H. Tost, H. Riede, A. Baumgaertner, S. Gromov, and B. Kern (2010), Development cycle 2 of the Modular Earth Submodel System (MESy2), *Geosci. Model Dev.*, *3*(2), 717–752, doi:10.5194/gmd-3-717-2010.
- Johnson, D. G., K. W. Jucks, W. A. Traub, and K. V. Chance (2000), Isotopic composition of stratospheric ozone, *J. Geophys. Res.*, *105*(D7), 9025–9031, doi:10.1029/1999JD901167.
- Johnston, J. C., and M. H. Thiemens (1997), The isotopic composition of tropospheric ozone in three environments, *J. Geophys. Res.*, *102*(D21), 25,395–25,404, doi:10.1029/97JD02075.

- Krankowsky, D., F. Bartheck, G. G. Klees, K. Mauersberger, K. Schellenbach, and J. Stehr (1995), Measurement of heavy isotope enrichment in tropospheric ozone, *Geophys. Res. Lett.*, *22*(13), 1713–1716, doi:10.1029/95GL01436.
- Krankowsky, D., P. Lämmerzahl, K. Mauersberger, C. Janssen, B. Tuzson, and T. Röckmann (2007), Stratospheric ozone isotope fractionations derived from collected samples, *J. Geophys. Res.*, *112*, D08301, doi:10.1029/2006JD007855.
- Liang, M.-C., G. A. Blake, and Y. L. Yung (2004), A semianalytic model for photo-induced isotopic fractionation in simple molecules, *J. Geophys. Res.*, *109*, D10308, doi:10.1029/2004JD004539.
- Liang, M.-C., F. W. Irion, J. D. Weibel, C. E. Miller, G. A. Blake, and Y. L. Yung (2006), Isotopic composition of stratospheric ozone, *J. Geophys. Res.*, *111*, D02302, doi:10.1029/2005JD006342.
- Mauersberger, K. (1981), Measurement of heavy ozone in the stratosphere, *Geophys. Res. Lett.*, *8*(8), 935–937, doi:10.1029/GL008i008p00935.
- Mauersberger, K., P. Lämmerzahl, and D. Krankowsky (2001), Stratospheric ozone isotope enrichments-revisited, *Geophys. Res. Lett.*, *28*(16), 3155–3158, doi:10.1029/2001GL013439.
- Miller, C. E., and Y. L. Yung (2000), Photo-induced isotope fractionation, *J. Geophys. Res.*, *105*(D23), 29,039–29,051, doi:10.1029/2000JD900388.
- Miller, C. E., R. M. Onorato, M.-C. Liang, and Y. L. Yung (2005), Extraordinary isotopic fractionation in ozone photolysis, *Geophys. Res. Lett.*, *32*, L1481, doi:10.1029/2005GL023160.
- Morton, J., J. Barnes, B. Schueler, and K. Mauersberger (1990), Laboratory studies of heavy ozone, *J. Geophys. Res.*, *95*(D1), 901–907, doi:10.1029/JD095iD01p00901.
- Ndengué, S. A., F. Gatti, R. Schinke, H.-D. Meyer, and R. Jost (2010), Absorption cross section of ozone isotopologues calculated with the multiconfiguration, *J. Phys. Chem.*, *114*, 9855–9863.
- Ndengué, S. A., R. Schinke, F. Gatti, H. D. Meyer, and R. Jost (2012), Ozone photodissociation: Isotopic and electronic branching ratios for symmetric and asymmetric isotopologues, *J. Phys. Chem. A*, *116*(50), 12,271–12,279.
- Ndengué, S., S. Madronich, F. Gatti, H.-D. Meyer, O. Motapon, and R. Jost (2014), Ozone photolysis: Strong isotopologue/isotopomer selectivity in the stratosphere, *J. Geophys. Res. Atmos.*, *119*, 4286–4302, doi:10.1002/2013JD020033.
- Nölscher, A. C., T. Butler, J. Auld, P. Veres, A. Muñoz, D. Taraborrelli, L. Vereecken, J. Lelieveld, and J. Williams (2014), Using total OH reactivity to assess isoprene photooxidation via measurement and model, *Atmos. Environ.*, *89*, 453–463, doi:10.1016/j.atmosenv.2014.02.024.
- Peeters, J., J.-F. Müller, T. Stavrou, and V. S. Nguyen (2014), Hydroxyl radical recycling in isoprene oxidation driven by hydrogen bonding and hydrogen tunneling: The upgraded LIM1 mechanism, *J. Phys. Chem. A*, *118*(38), 8625–8643, doi:10.1021/jp5033146.
- Sander, R., P. Jöckel, O. Kirner, A. T. Kunert, J. Landgraf, and A. Pozzer (2014), The photolysis module JVAL-14, compatible with the MESSy standard, and the JVal PreProcessor (JVPP), *Geosci. Model Dev.*, *7*(6), 2653–2662, doi:10.5194/gmd-7-2653-2014.
- Sander, S. P., et al. (2011), Chemical kinetics and photochemical data for use in atmospheric studies. Evaluation number 17. NASA Panel for Data Evaluation No. 17, JPL Publ. 10–6, Jet Propul. Lab., Pasadena. [Available at <http://jpldataeval.jpl.nasa.gov>.]
- Schinke, R. (1993), *Photodissociation Dynamics*, *Cambridge Monographs on Atomic, Molecular and Chemical Physics 1*, 412 pp., Cambridge Univ. Press, Cambridge.
- Schmidt, J. A., M. S. Johnson, and R. Schinke (2011), Isotope effects in N<sub>2</sub>O photolysis from first principles, *Atmos. Chem. Phys.*, *11*, 8965–8975, doi:10.5194/acp-11-8965-2011.
- Schmidt, J. A., M. S. Johnson, and R. Schinke (2013), Carbon dioxide photolysis from 150 to 210 nm: Singlet and triplet channel dynamics, UV-spectrum, and isotope effects, *PNAS*, *110*(44), 17,691–17,696, doi:10.1073/pnas.1213083110.
- Taraborrelli, D., M. G. Lawrence, J. N. Crowley, T. J. Dillon, S. Gromov, C. B. M. Grosz, L. Vereecken, and J. Lelieveld (2012), Hydroxyl radical buffered by isoprene oxidation over tropical forests, *Nat. Geosci.*, *5*(3), 190–193, doi:10.1038/ngeo1405.
- Thiemens, M. H., and T. Jackson (1990), Pressure dependency for heavy isotope enhancement in ozone formation, *Geophys. Res. Lett.*, *17*(6), 717–719, doi:10.1029/GL017i006p00717.
- Vicars, W. C., and J. Savarino (2014), Quantitative constraints on the 17O-excess ( $\Delta 17\text{O}$ ) signature of surface ozone: Ambient measurements from 50°N to 50°S using the nitrite-coated filter technique, *Geochimica et Cosmochimica Acta*, *135*, 270–287, doi:10.1016/j.gca.2014.03.023.